Journal of Materials Chemistry B

ROYAL SOCIETY OF CHEMISTRY

PAPER

View Article Online
View Journal | View Issue

Cite this: J. Mater. Chem. B, 2020, 8, 7966

Leucine-activated nanohybrid biofilm for skin regeneration *via* improving cell affinity and neovascularization capacity

Xiajie Lin,[a] Yamin Li,[b] Wei Luo,[a] Lan Xiao,[cd] Zeren Zhang,[a] Jinzhong Zhao, *[b] Changsheng Liu *[a] and Yulin Li *[a]

Received 11th April 2020,
Accepted 15th July 2020

DOI: 10.1039/d0tb00958j

rsc.li/materials-b

The accumulation of skin diseases has increased the need for biomimicking materials with high bioactivity and biosafety for wound healing, where how to improve the cell affinity of the skin regenerative materials as well as their neovascularization capacity is a key factor for rapid regeneration of the injured skin tissue. In the current study, we developed an advanced type of biodegradable nanofibrous biofilm which can attract skin-related cells and accelerate blood vessel formation for skin regeneration. Firstly, bioactive nanohybrids (LEU@LP) were fabricated *via in situ* doping of the nutrient amino acid leucine (beneficial for fibroblast proliferation and protein synthesis) into LAPONITE® nanodisks (enriched in Mg and Si favorable for vascularization). LEU@LP nanoparticles were then hybridized with a biodegradable polylactide (PLA) nanofibrous mesh *via* an airbrushing technique, followed by a subsequent ammonia plasma surface treatment to improve PLA's hydrophilicity to increase cell affinity. The resulting hybrid biofilms with skin-biomimicking nanofibrous structural networks can promote cell adhesion, spreading, migration and proliferation of fibroblasts, leading to the ideal skin wound healing (with blood vessel formation and hair follicle regeneration), probably attributed to their better hydrophilicity to promote cell affinity and the capacity of sustainable release of leucine (beneficial for fibroblasts proliferation) and the composition provision (Mg and Si which are beneficial for neovascularization).

Introduction

Skin loss and dysfunctions due to wounds, trauma, burns, aging, and surgery could result in amputation or other life-threatening consequences, which greatly affect human health.[1–4] Autografts, allografts and artificial implants are general methods for the regeneration of skin. The problems with autografts are the limited resources and unavoidable injury and complications with graft-tissue harvesting, and the drawbacks of allografts, such as immune rejection and virus-inducing risks, suggesting both these methods are unsatisfactory for clinical needs.[5] Although various natural-derived polymeric grafts[6,7] (*e.g.*, fibrin,[8] gelatin,[9] elastin,[10] chitosan[11]) with compositional biomimicry properties have been developed and used at the clinical level,[12,13] their animal origin, uncontrolled structure and mechanical brittleness have been found to cause serious problems, such as limited cells/nutrient/mass transportation problems and immunogenic risk. These disadvantages greatly hamper their biomedical applications,[5] and they are mainly used as auxiliary materials to clean wounds, absorb tissue exudate and protect wounds.[14] Therefore, how to develop artificial grafts with high bioactivity and biosafety is a crucial and challenging issue for skin regeneration in the field of modern regenerative medicine. To solve this problem, researchers have developed natural polymers, synthetic polymers, or a combination of two, such as chitosan,[15] collagen,[16] poly(lactic-*co*-glycolic acid),[17] poly(ε-caprolactone),[18] and polylactide,[19] to synthesize different forms of smart dressings. The advantages of polylactide, such as its biodegradability and controllable structure make it widely used in the field of biomedicine, and it has been used as a bulk material to obtain smart dressings in the form of thin films,[20] nanosheets,[21] nanoparticles,[22] *etc.*, to develop a device for growth factor and cell delivery. In addition, a variety of functionalization methods have been applied to modify the dressing,[23] including doping, copolymerization, and a series of surface functionalization strategies.

[a] The Key Laboratory for Ultrafine Materials of Ministry of Education, State Key Laboratory of Bioreactor Engineering, Engineering Research Center for Biomedical Materials of Ministry of Education, School of Materials Science and Engineering, East China University of Science and Technology, 200237, Shanghai, China. E-mail: liucs@ecust.edu.cn, yulinli@ecust.edu.cn
[b] Shanghai Jiao Tong University Affiliated Sixth People's Hospital, 200233, Shanghai, China. E-mail: jzzhao@sjtu.edu.cn
[c] Institute of Health and Biomedical Innovation, Queensland University of Technology, Brisbane, QLD 4059, Australia
[d] The Australia-China Centre for Tissue Engineering and Regenerative Medicine (ACCTERM), Brisbane, QLD 4059, Australia

Wound healing is a complicated process generally consisting of four successive and overlapping steps: (1) hemostasis phase; (2) inflammatory phase; (3) proliferative phase; and (4) maturation and remodeling phase.[24,25] As skin-related cells, fibroblasts are one type of critical cell at the proliferative phase, and participate in many important biological activities during the wound healing process, including protein synthesis, activating bioactive signaling for new skin tissue formation and vascularization.[5,26–29] For instance, during the formation of granulation tissue, fibroblasts are stimulated and then migrate into the wound site, then proliferate to reconstruct various connective tissue components.[26] Furthermore, fibroblasts are responsible for the synthesis of extracellular matrix (ECM) proteins, which are beneficial to construct homogeneous microenvironments with special constituents (*e.g.*, collagen and other related proteins) and different bioactive factors to facilitate vascularization, thereby maintaining good blood balance and sufficient nutrient/mass provision[27] for guidance of skin regeneration.[5,28,29] Hence, the biomimetic materials should be designed with good cell affinity and neovascularization ability, which can recruit fibroblasts and regulate their ECM protein synthesis behaviors, thereby achieving effective wound healing in the skin tissues.

As a bioactive amino acid, leucine is involved in multiple human biological activities, such as protein synthesis,[30] weight reduction[31] and muscle regeneration.[32] For instance, leucine can promote the absorption of glucose and increase the sensitivity of insulin to maintain the blood glucose balance;[33–35] this energetic process is helpful to accelerate the fat burning effect for body building.[36,37] The lack of leucine may cause hypoglycemia-related diseases, including headache, fatigue, depression, insanity, and irritability.[38] Recent reports indicated that leucine may stimulate protein synthesis by improving the expression of eukaryotic initiation factors and down-regulate the proteolysis by inhibiting ATP ubiquitin-proteasome pathways.[39] When leucine is combined with sestrin2, the mTORC1 complex expression will be activated in fibroblasts,[40] which is beneficial to the proliferation of fibroblasts and increase in contractile α-smooth muscle actin expression, enabling their potential in wound healing applications.[3,39] Despite these benefits, the use of too much leucine may cause high side effects, such as pellagra[41] and dermatitis.[42] Therefore, it is necessary to develop a kind of material which can sustainably deliver leucine to maximize its benefits for skin regeneration *via* improving its instability and avoiding side effects.

Herein, we proposed to develop a biodegradable wound healing film, which can act as a leucine reservoir for the sustainable delivery of this signaling molecule in order to accelerate the proliferation of fibroblasts and to promote their protein synthesis for skin regeneration. We firstly fabricated a type of leucine-carrying nanohybrid by *in situ* encapsulating it in a kind of silicate-based nanodisk (LAPONITE®, LP) containing Mg and Si to promote the formation of neovascularization.[43,44] The leucine-loaded nanohybrids were then *in situ* doped into the biodegradable nanofibrous biofilm of polylactide (PLA, a kind of biodegradable polymer approved by the Food and Drug Administration (FDA)[45]) *via* an airbrushing technology (a simple and effective nanofiber-spinning technique as compared to the electrospinning method[46]) to form an ECM-mimicking nanofibrous architecture.[47,48] The obtained hybridized biofilms subsequently underwent ammonia plasma surface treatment to increase the PLA's hydrophilicity to improve its cell affinity.[46] We found that the leucine-incorporated LP-hybridized biofilms with biodegradability and biosafety could comprehensively promote wound healing effects by synergistically improving their cell affinity as well as neovascularization capacity, at both *in vitro* and *in vivo* levels (Scheme 1).

Results and discussion

Preparation and characterization of LEU@LP nanohybrids

The instability and side effects of small molecular therapeutic agents are the main problems for their biomedical applications.[49] To overcome these disadvantages, we firstly developed a kind of nanocarrier for leucine delivery *via* a simple assembly of the drug onto silicate-based nanodisks (LAPONITE®, LP) enriched in Mg and Si components with a potential to promote neovascularization.[43,44] The morphology of the resulting nanohybrids (LEU@LP) was firstly observed under a transmission electron microscope (TEM). As shown in Fig. 1B, LEU@LP had a nanosize of 32.2 ± 4.2 nm, which was a little bigger than the original nanosize of LAPONITE® (22.2 ± 2.5 nm in diameter[50]). The microstructure of the resulting nanohybrids was characterized by FTIR analysis. Similar to LP, LEU@LP nanoparticles offered characteristic peaks at 1006 cm^{-1} corresponding to the stretching vibration of the Si–O and Si–O–Si bands, and at 3431 cm^{-1} corresponding to the –OH bending bonds.[51] Meanwhile, different from native LP, the LEU@LP nanoparticles also displayed some new absorption peaks at 768 cm^{-1} and 1610 cm^{-1}, which may come from the vibration bands of the –NH group and –COOH group of the leucine molecule,[52] respectively. The new FTIR peak appearance in LEU@LP indicated a successful loading of leucine into LP, resulting in the nanosize increase after the assembly of LP with the leucine (Fig. 1C).

Preparation and characterization of hybridized nanofibrous biofilms

In tissue engineering, it is important to develop bioactive materials with a structure mimicking that of the specific tissue to be regenerated.[53] Since skin tissue owns a nanofibrous collagen network architecture, we developed biodegradable ECM-mimicking nanofibrous films of polylactide (PLLA, a kind of FDA-approved biodegradable polymer)[45] *via* an airbrushing technology (a simple and effective nanofiber-spinning technique as compared to electrospinning method[46]), through which LEU@LP nanoparticles were *in situ* doped with pure PLLA matrix to increase its bioactivity. The morphology and structure of the airbrushed films were characterized by scanning electron microscopy (SEM). As shown in Fig. 2, all the films assumed a nanofibrous structure. The native PL film had nanofibers with a diameter of 227.0 ± 8.0 nm, while the hybridized films had larger nanofiber sizes (238.9 ± 7.7 nm for the PLP film,

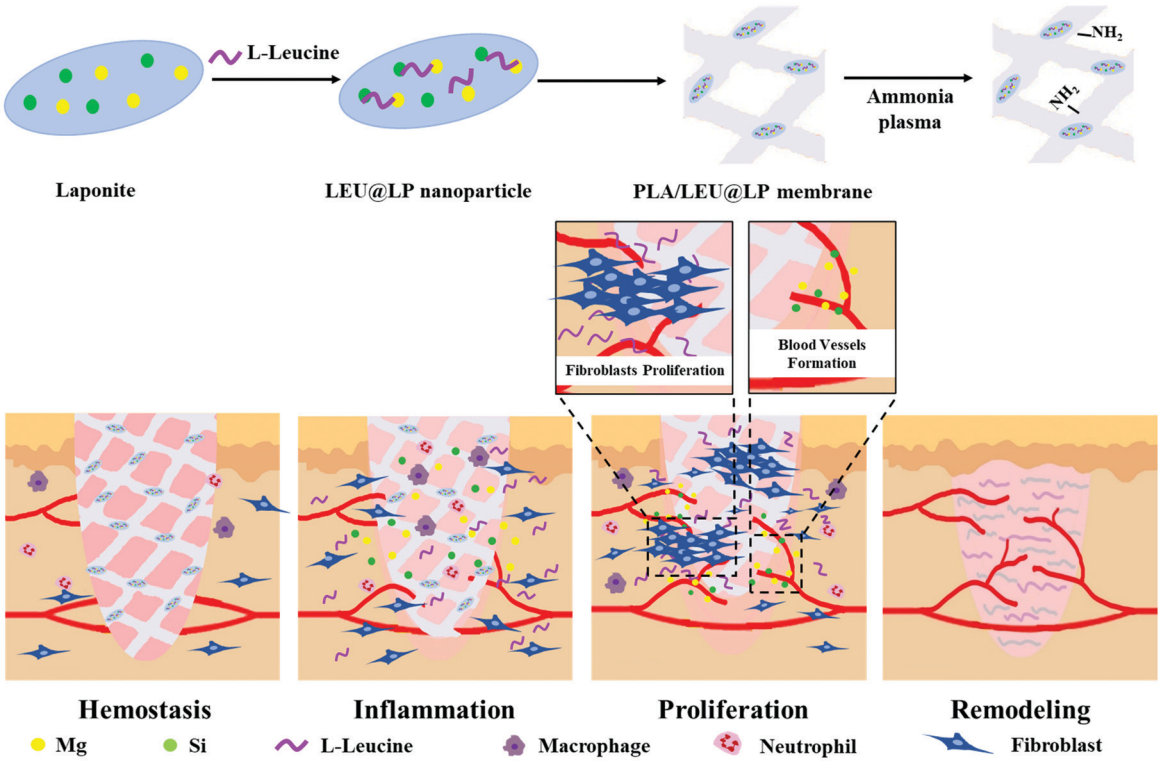

Scheme 1 The schematic diagram of the fabrication of the nanofibrous film and its capacity for the promotion of wound healing. The ECM-mimicking structure of the biofilm and its improved hydrophilicity may benefit cell adhesion, spreading and proliferation. During the proliferation phase of wound healing, the hybrid biofilm can maintain a sustained release of leucine (to stimulate the proliferation of fibroblasts) as well as that of the silicon and magnesium elements from LAPONITE® to induce the formation of blood vessels, which together accelerate wound healing efficacy.

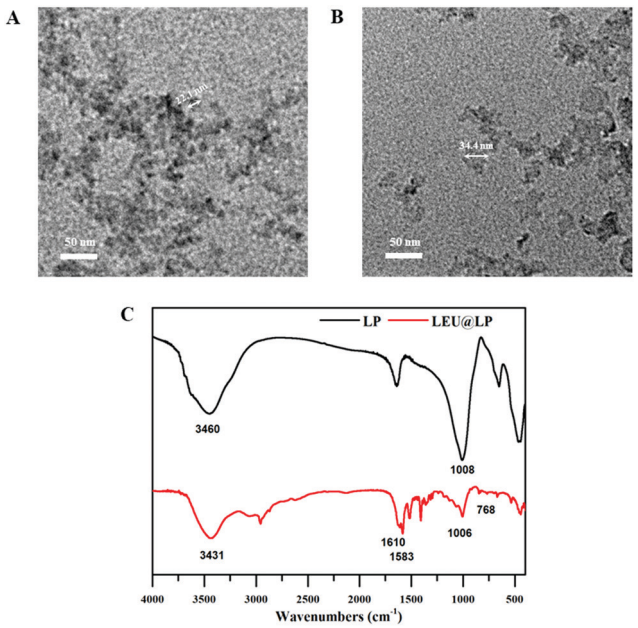

Fig. 1 TEM micrographs of the (A) LP particles and (B) LEU@LP particles. (C) FTIR spectra of LP and LEU@LP particles.

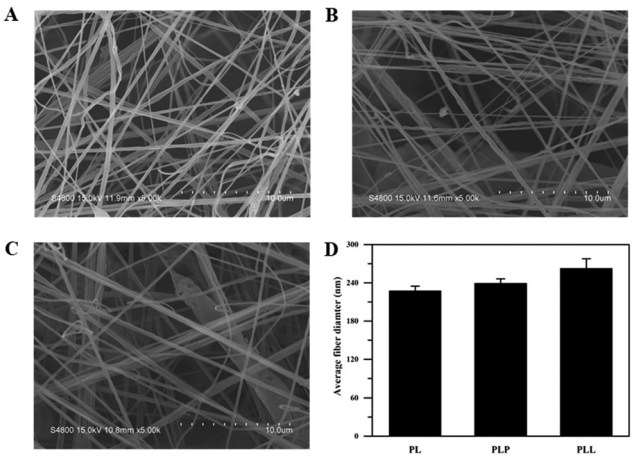

Fig. 2 SEM micrographs of the nanofibrous films: (A) PL film, (B) PLP film, (C) PLL film, and (D) the average nanofiber diameters of the films (PL, PLP and PLL).

and 262.1 ± 15.6 nm for the PLL film), suggesting the successful hybridization of the nanoparticles into the biodegradable films *via* the airbrushing spinning method.

The PLL biofilm was further investigated by an energy-dispersive spectroscopy analysis technique (EDS) coupled with a scanning electron microscope. It can be observed from Fig. 3, that the hybrid biofilm presented EDS mapping images clearly indicated the presence of silicon (Fig. 3A), magnesium (Fig. 3B), and nitrogen elements (Fig. 3C). Among them, the silicon and magnesium compositions should come from the silicon and magnesium enriching LAPONITE® nanodisks, while the

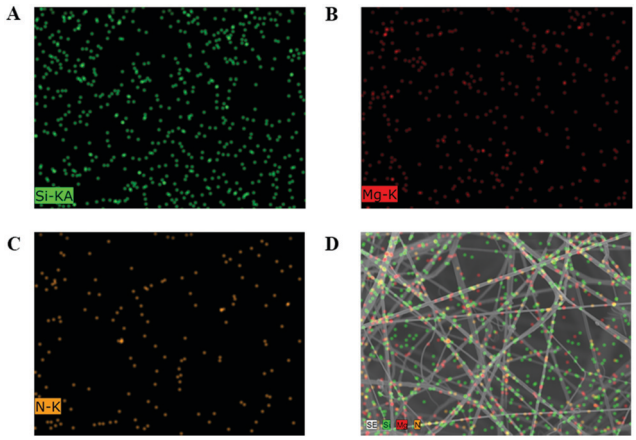

Fig. 3 The energy-dispersive spectroscopy (EDS) images of PLL biofilms: (A) silicon (Si), (B) magnesium (Mg), and (C) nitrogen (N) elements. (D) The merged images of the above three elements with the normal SEM image of the PLL biofilm.

nitrogen component may come from the leucine hybridized in the biofilm (Fig. 3C). The merged SEM image demonstrated that the components were well distributed along the nanofibrous fibers (Fig. 3D), again suggesting a successful homogeneous hybridization of LEU@LP nanoparticles into the nanofibrous films *via* the airbrushing technique.

From the FTIR results in Fig. 4, it could be observed that before ammonia plasma treatment, the infrared of the PLP and PLL spinning membrane was basically the same as that of the pure PL spinning membrane, and 1090 cm^{-1} and 1750 cm^{-1} corresponding to the C–O vibration peak and C═O vibration peak of polylactide,[54] probably due to the doped LP and LEU@LP nanoparticles wrapped in biofilms. This is also consistent with the phenomenon that the water contact angles of membranes were close before the plasma treatment. It is known that, as well as the surface topographical morphology, the hydrophobic or hydrophilic features of the substrate also play an important role on the regulation of the cell behaviors (*e.g.*, cell attachment, spreading and proliferation[55,56]). Due to their good biocompatibility, biodegradability and controllable structure, polylactide-based polymers have been clinically used for tissue engineering and drug delivery, while their poor hydrophilicity is the major drawback limiting their further biomedical applications.[46] In order to solve this problem, we next used the ammonia plasma surface treatment technique to increase its hydrophilicity (to introduce amino groups onto the biofilm surface). The hydrophilicity of the nanofibrous biofilms was examined *via* water contact angle analysis. As shown in Fig. 4B, the biofilms in the absence of plasma surface treatment presented a high water contact angle (136.7 ± 3.9°, 131.9 ± 3.0° and 136.8 ± 2.6° for the PL, PLP, and PLL films, respectively), while the plasma treatment dramatically reduced the water contact angles (89.0 ± 2.7°, 83.25 ± 6.9° and 24.7 ± 0.6° for the PLt, PLPt, and PLLt films, respectively). These data indicate that the plasma treatment effectively increased the hydrophilicity of the nanofibrous films, probably because the ammonia plasma treatment is helpful to introduce some hydrophilic nitrogen-containing group (*e.g.*, amines, imines) onto the nanofibrous films, which can be supported by the significant nitrogen content increase in the hybrid biofilm after surface treatment (Fig. 5). Since the PLL film itself contains leucine with a nitrogen element, the same plasma treatment resulted in an optimal improvement of its hydrophilicity (water contact angle: 24.7 ± 0.6°) which is beneficial to cell affinity.[55] As such, our results indicate that LEU@LP-incorporated PLL nanofibrous biofilms with good surface hydrophilicity have been successfully developed, where the LP components can act as a nano-reservoir for sustainably providing both silicon and magnesium (to promote neovascularization[43,44]) as well as bioactive leucine amino acid (to enhance fibroblast proliferation). The incorporation of the bioactive motifs, together with their good hydrophilicity (to increase cell affinity), is expected to create appropriate microenvironments to recruit targeted skin-related cells and to guide and promote cell attachment, spreading, proliferation, as well as neovascularization, benefiting the healing process of wounds or degenerative skin tissues.

Biocompatibility is necessary for materials to be used in the biomedical field.[57] Since fibroblasts are skin-repairing cells, a fibroblast cell line (L929 cells) was used for *in vitro*

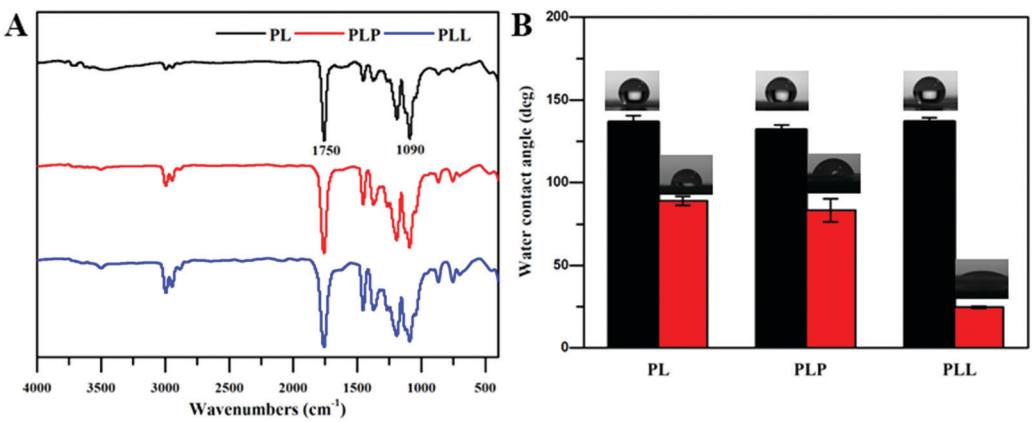

Fig. 4 (A) FTIR spectra of PL, PLP and PLL films. (B) The water contact angles of the nanofibrous films before (PL, PLP, PLL) and after (PLt, PLPt, PLLt) plasma surface treatment.

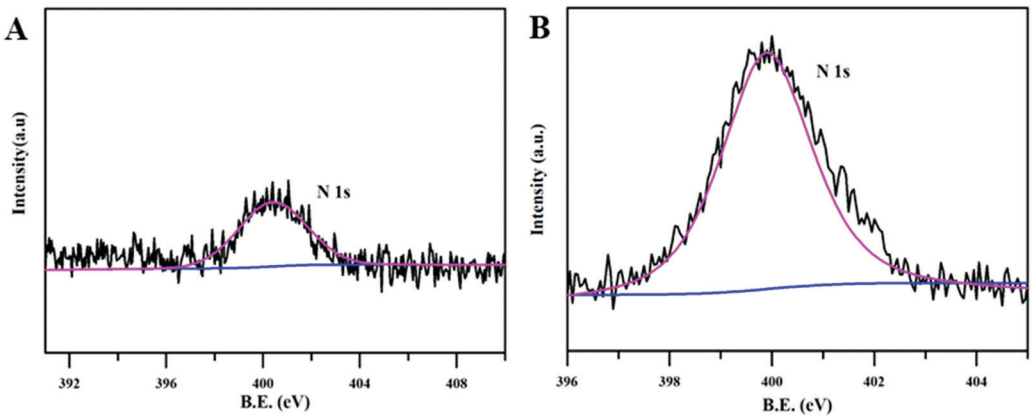

Fig. 5 XPS scanning of the PLL film. (A) The narrow scan of nitrogen element of the PLL film. (B) The narrow scan of nitrogen element in the PLLt film.

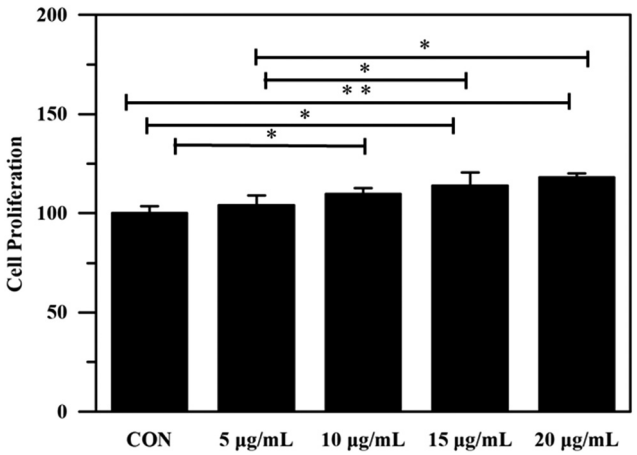

Fig. 6 Cell proliferation of L929 cells cultured with LEU@LP nanoparticles for 2 d. (*$p < 0.05$, **$p < 0.01$).

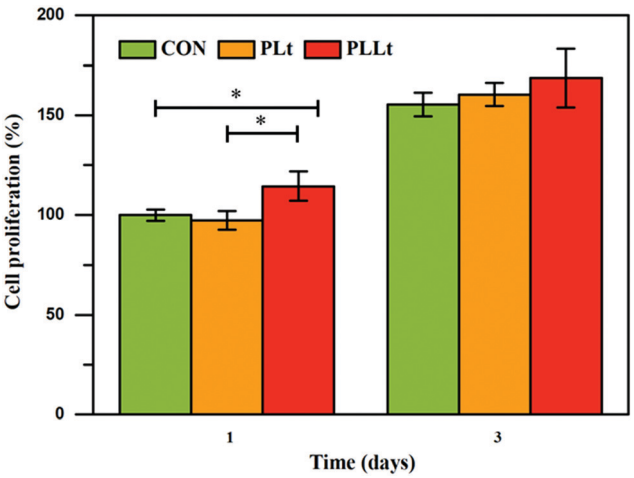

Fig. 7 Cell proliferation of L929 cells cultured with PLt and PLLt films for 1 d and 3 d. (*$p < 0.05$).

biocompatibility examination *via* 3-(4,5-dimethylthiazol-2-yl)-2,5-diphenyltetrazole bromide (MTT) assay. As shown in Fig. 6, after 2 d incubation, all cells treated with LEU@LP nanoparticles (with a concentration up to 20.0 μg mL^{-1}) presented over 100% cell viability, suggesting the good biocompatibility of LEU@LP nanoparticles. Notably, the increase of the LEU@LP concentration from 0 to 20.0 μg mL^{-1} led to a continuous cell proliferation increase, indicating the positive effects of the LEU@LP nanoparticles on cell growth, probably due to the nanohybrid-derived bioactive leucine amino acid, which could promote fibroblast proliferation.

To evaluate the effects of the biofilm on fibroblast proliferation, we next examined the proliferation of L929 cells cultured on the nanofibrous biofilms by MTT assay. As shown in Fig. 7, after 1 d incubation, the PLLt biofilms presented cell viability of no less than 100%, indicating their good biocompatibility.[58,59] The PLLt film presented a higher cell viability (114.4 ± 7.3%) than the DMEM control and PLt films, which may be associated with the incorporation of LEU@LP nanohybrids into the PLA film to facilitate the proliferation of fibroblasts (Fig. 6). With 3 d incubation, all the films obviously accelerated the proliferation of L929 cells, probably because the films owned ECM-mimicking nanofibrous porous architecture and large surface area which are beneficial to cell adhesion, spreading and growth.[60] Compared to other groups after 3 d incubation, the LEU@LP-doped hybrid film offered higher cell proliferation capacity, probably because they had better hydrophilicity[61] which is beneficial to cell affinity, and contained LEU@LP nanocarriers, which can sustainably provide a bioactive composition favorable to promote the proliferation of fibroblasts.[62]

Cell morphology is closely related to cell functions (*e.g.*, cell proliferation, differentiation, and apoptosis). The lack of cell-material interactions may result in poor cell attachment, eventually causing cell apoptosis.[5] In order to observe cell morphology in the spinning film, L929 cells on the film were firstly stained with FITC, and then observed by laser scanning confocal microscopy and scanning electron microscopy. As shown in Fig. 8A and B, compared to the pure PLt film, L929 cells cultured on the PLLt film presented better cell attachment and higher cell density with spindle-shaped expanded shapes. The above cell proliferation data and the morphological images clearly indicated that the PLLt biofilm could promote cell

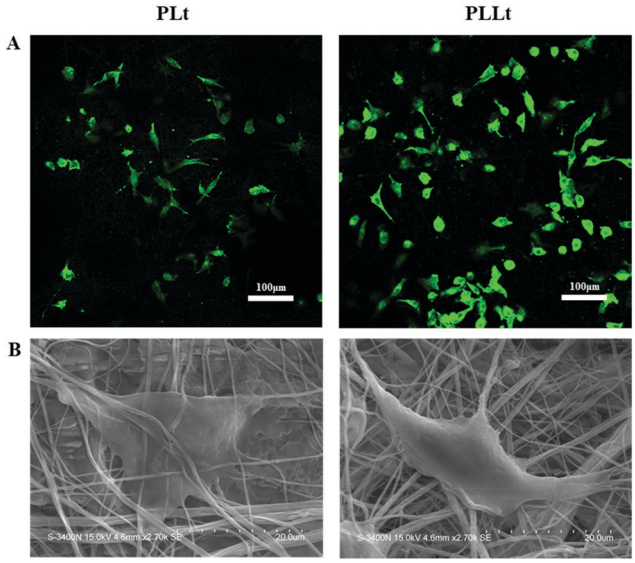

Fig. 8 (A) Fluorescent images of L929 cells on PLt and PLLt films for 24 h incubation. (B) SEM images of L929 cells on PLt and PLLt films after 24 h incubation.

adhesion, spreading and growth. These significantly-improved cell activities from the PLLt film may be due to its ECM-mimicking nanofibrous architecture (beneficial to protein adsorption), good hydrophilicity (to increase cell affinity), and enriching bioactive ingredients (Mg, Si, and leucine components favorable for cell proliferation and protein synthesis (Fig. 7 and 8)).

For wound healing treatment, it is important to attract skin-related cells to the injury site in a timely manner, and cell migration is a key factor representing the cell recruitment efficiency of the material. Therefore, we next constructed a cell scratch model for the investigation of the cell migration behaviors of fibroblasts. As shown in Fig. 9, after 24 h incubation, the scratch space of the PLLt film was almost covered with L929 cells with higher cell density as compared to the DMEM control and pure PLt film. The induced cell migration of the PLLt biofilm may be ascribed to the released effective bioactive ingredients. In addition, the nanofibrous structure and good hydrophilicity of the films may further promote cell adhesion, migration and proliferation, thereby potentially accelerating the wound healing process.[63,64]

To evaluate the wound healing effects of the nanofibrous films, two circular skin wounds (5 mm diameter) were created on the back of each mouse and covered with the biodegradable films (PLPt film and PLLt film) of the same size on the skin defect (no material wound served as the blank control). Fig. 10 shows the wounds treated for different periods of time. Although all the wound areas gradually decreased from 0 to 14 d, the PLLt biofilm obviously accelerated the wound healing

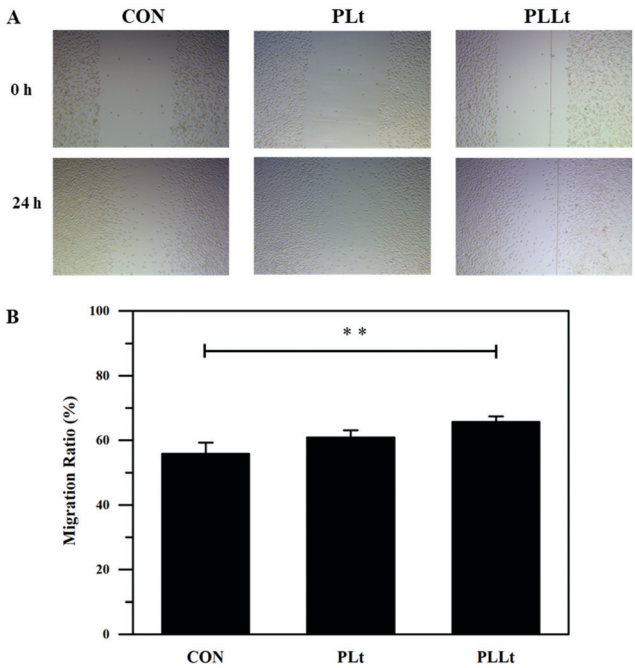

Fig. 9 Cell migration behaviors of the L929 cells. (A) Images of cell migration after 24 h treatment with the extract solution of the biofilms (PLt and PLLt), and (B) their corresponding migration ratio. (**$p < 0.01$).

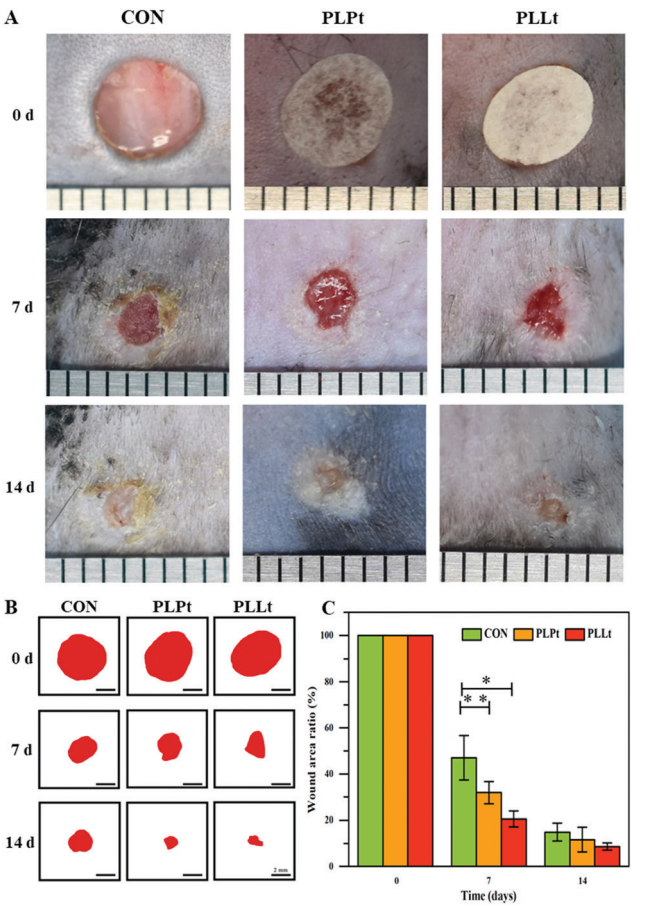

Fig. 10 Wound healing evaluation of the mice after *in vivo* treatment with the nanofibrous films (PLPt and PLLt films) for 7 d and 14 d: (A) the digital photos of the wound areas of the mice after 7 d and 14 d treatment, (B) the simulated unhealed skin areas of the mice after 7 d and 14 d treatment, and (C) the unhealed ratios of the mice after 7 d and 14 d treatment. (*$p < 0.05$, **$p < 0.01$).

process as compared to the PLPt film group and the blank control group up to a period of 14 d treatment (Fig. 10A–C).

For the observation of general morphology, the regenerated skin tissues were harvested from the mice after 14 d treatment, and were sliced and stained with hematoxylin and eosin (H&E), followed by imaging with a light microscope. As shown in Fig. 11A, after 14 d treatment, a new epidermis layer was formed on all the newly formed skin. Furthermore, different from the control and PLPt group, dermal and epidermal structures were more complete in the PLLt film group, allowing for the deposition of denser orientated collagen, formation of blood vessels and skin appendages (*e.g.*, hair follicles). During wound healing, fibroblasts convert into myofibroblasts and synthesize type I and type III collagen. With the progression of wound maturity, type III collagen is converted to type I collagen to increase the interaction between the newly formed fibers.[65] From the immuno-histochemistry image (Fig. 11B), it can be observed that compared with the control group, the expression of type I collagen is induced in the PLPt and PLLt groups. In addition, the PLLt group showed a more orderly fiber sorting, indicating that these biofilms played a role in the collagen enhancement process. Angiogenesis is a vital part of wound healing. In this study, immuno-histochemistry staining against CD31 (a marker for endothelial cells[66]) was performed to evaluate angiogenesis *in vivo*. From the results of Fig. 11C, $CD31^+$ tube-like structures could be observed, which in combination with the H&E staining results (Fig. 11A), suggests there are more newly formed blood vessels in the PLLt and PLPt treatment groups. Compared with the control group, the new blood vessels in the PLLt group showed a uniform tube. These results indicate that PLLt and PLPt biofilms can stimulate angiogenesis during wound healing.

As such, all biological experimental results indicated that the LEU@LP-doped nanofibrous biofilm (PLLt) exerted an optimal wound healing efficacy, probably due to the bioactive components (Mg, Si and leucine) and good hydrophilicity of the PLLt film, which can promote the cell affinity (adhesion and adhesion) of the skin related cells (endothelial cells, fibroblasts, keratinocyte), and adjust cell rhythm (migration and spreading), leading to acceleration of cell proliferation as well as neovascularization for ideal skin wound healing, including important skin appendages (*e.g.*, hair follicles).[67] The combinative merits of the PLLt biofilms can be outlined as follows: firstly, we used the ammonia plasma surface treatment to greatly improve the hydrophilicity of the hybrid nanofibrous film, which should be beneficial for cell affinity, attachment, spreading, migration and proliferation of the skin regeneration related cells (endothelial cells, fibroblasts, keratinocyte).

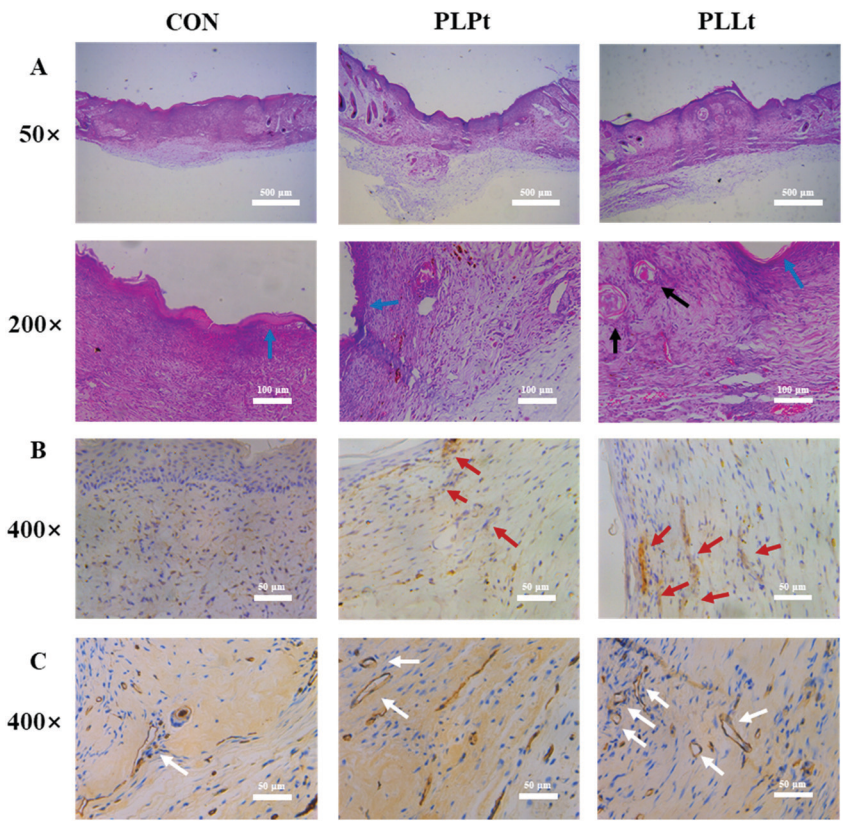

Fig. 11 General morphology, type I collagen and CD 31 expression of the repaired skin tissues from the mice treated with PLPt and PLLt nanofibrous films for 14 d (blue arrows: epidermis; black arrows: hair follicles; red arrows: type I collagen; white arrows: blood vessels): (A) the representative H&E staining sections images, (B) the representative immuno-histochemistry (IHC) staining images of collagen I, and (C) the representative IHC staining images of CD 31.

Secondly, the hybrid biofilm contained LEU@LP nanohybrids, which can sustainably release the bioactive leucine amino acid with the ability to promote the proliferation of fibroblasts and their protein synthesis. Thirdly, the hybrid film can offer a continuous delivery of Mg and Si components to induce the formation of new blood vessels, thereby maintaining blood and oxygen balance for skin regeneration in a timely manner. The synergistic materiobiological effects[5] together with the good biocompatibility and controllable biodegradability, endowed the biofilm with nearly perfect skin wound healing efficacy *via* accelerating cell proliferation, neovascularization and regeneration of the important skin appendages (*e.g.*, hair follicles).[67]

Conclusions

In summary, we developed a facile approach to fabricate a kind of bioactive hybrid nanofibrous biofilm (PLLt) for skin regeneration. Bioactive nanohybrids (LEU@LP) were prepared *via* self-assembly of leucine (favorable for the proliferation of fibroblasts) into LAPONITE® (LP) nanodisks. The LEU@LP nanocarriers were then *in situ* doped into the polylactide matrix to offer a kind of bioactive and biodegradable film using an airbrushing technique, followed by ammonia plasma surface treatment. The hybridized nanofibrous films presented a nanofibrous network and enhanced hydrophilicity. Biological evaluation indicated that the developed hybrid biofilm exhibited good cell affinity (cell adhesion and spreading) to enhance the proliferation of skin-related cells and promoted neovasculation to achieve ideal skin wound healing (including hair follicle regeneration), which are probably associated with the good ECM-mimicking nanofibrous structure (favorable protein adsorption), sustainable release of bioactive leucine (beneficial to the proliferation of fibroblasts) and element constituents (Mg and Si which are beneficial to new blood vessel formation) of this hybrid film. Our study therefore potentially provides an advanced therapeutic tool for skin regeneration, which sheds light on the field of regenerative medicine.

Experimental section

Materials

LAPONITE® (LP) was offered from Rocwood Additives Limited, UK. L-Leucine was obtained from Aladdin Biochemical Technology Co., Ltd (Shanghai, China). 3-(4,5-Dimethyl-2-thiazolyl)-2,5-diphenyl-2-*H*-tetrazolium bromide (MTT) was received from Life Technology (Carlsbad, USA). Dichloromethane and ethanol were purchased from Titan Technology Co., Ltd (Shanghai, China). Hydrochloric acid was bought from Lingfeng Chemical Reagent Co., Ltd (Shanghai, China). Poly(L-lactic acid) (PLLA) was synthesized by our laboratory.[46] Mouse fibroblast cell lines (L929 cell) were purchased from the cell bank of Chinese Academy of Sciences (Shanghai, China). All other reagents were of analytical grade and used without further purification.

Fabrication of leucine/LAPONITE® nanohybrids (LEU@LP)

0.1 g of LAPONITE® was dispersed in 5.0 mL of distilled water under 10 min sonication, followed by the addition of 0.1 M HCl to adjust the pH value to 3.0. After that, 5.0 mL of an aqueous solution of L-leucine (0.4 M) was dropwise added to the above solution. After 24 h of magnetic stirring, the mixture underwent lyophilization to offer Leucine/LAPONITE® nanohybrids (LEU@LP).

Preparation of the nanohybridized biofilms and their surface plasma treatment

1 g of PLLA, PLLA/LP, or PLLA/LEU@LP (the amount of LP was maintained at 2.0 wt%) was dissolved in a mixture of dichloromethane and ethanol (volume ratio: 95 : 5) under magnetic stirring for 4 h (PLLA concentration: 30 mg mL^{-1}). The solutions were airbrushed into nanofibrous biofilms on a commercial airbrush (HD-130, Syou Tools, China) equipped with a 0.5 mm-diameter nozzle under 0.2 MPa gas flow pressure at a 20 cm nozzle-receiver distance. The nanofibrous biofilms were dried in a vacuum oven at 37 °C for 24 h to offer PLLA, PLLA/LP, and PLLA/LEU@LP biofilms (abbreviated as PL, PLP and PLL, respectively). For surface treatment, the biofilms were placed in the chamber of a plasma cleaner at a power of 50 W for 30 s under an atmosphere of ammonia gas, to obtain the treated biofilms, which were abbreviated as PLt, PLPt and PLLt, respectively.

Morphological characterization of the nanoparticles and biofilms

The morphology of the nanohybrids was examined using a transmission electron microscope (TEM, JEM-1400, Japan). Before measurement, an aqueous solution of nanoparticles was dropped onto a copper grid and air-dried. A field emission scanning electron microscope coupled with an energy dispersive spectrometer (FESEM, Hitachi S-4800, Japan) was used for morphological observation and elemental analysis of the biofilms under an acceleration voltage of 15 kV. The biofilms were sprayed with gold for 50 s before measurement.

Flourier transformed infrared (FTIR) and surface X-ray photoelectron spectroscopy (XPS) characterization of nanoparticles and biofilms

The nanohybrids were prepared *via* a KBr tableting method and measured by FTIR spectroscopy (Nicolet 5700, Thermo, USA), while the biofilms were investigated through attenuated total reflection FTIR in the wavelength range of 4000–400 cm^{-1}. The biofilms also underwent surface element analysis using an X-ray photoelectron spectroscopy instrument (ESCALAB 250Xi, Thermo, USA) with Al Kα radiation.

Water contact angle measurement of nanofibrous biofilms

The water contact angle of the nanofibrous biofilms was characterized using a contact angle meter (JC2000D2, Zhongchen Instruments, China) and imaged using a digital camera.

In vitro biological evaluation

For the study of the bioactivity of LEU@LP nanohybrids, 100 μL of L929 cell solution with a density of 5.0×10^3 cells per well was seeded into a 96-well plate and incubated in a 37 °C incubator for 24 h. Then, the medium was replaced with LEU@LP solution at different concentrations (0, 5.0, 10.0, 15.0 and 20.0 μg mL^{-1}) diluted by Dulbecco's modified Eagle's medium (DMEM) containing 10% Gibco serum. After 48 h, 30 μL of MTT solution (5.0 mg mL^{-1}) was added to each well, and the culture was continued for 4 h. After that, the medium was exchanged with 200 μL of DMSO solution to completely dissolve the crystals by shaking for 15 min. The solution was placed on a microplate reader (SPECTRAmax 384, Molecular Devices, USA) to measure the absorbance at a wavelength of 492 nm. The cell proliferation was calculated by the following equation:

$$\text{Cell viability (\%)} = OD_{sample}/OD_{control} \times 100\%$$

To investigate their biocompatibility, the round nanofibrous films with a diameter of 15 mm were placed in a 24-well plate, and then sterilized by ultraviolet irradiation for 24 h. 1 mL of L929 cell solution at the density of 2.0×10^4 cells per well were seeded into the above PLt and PLLt film and placed in an incubator at 37 °C for 24 h and 72 h, respectively, followed by MTT assay using a method similar to the above.

For the cell morphology study, L929 cells were seeded on the sterilized films at a cell density of 2.0×10^4 cells per well in a 37 °C incubator. After 24 h culture, the cells were washed with PBS 3 times and fixed with glutaraldehyde (2.5%) for 15 min at room temperature, followed by cell cytoskeleton staining using FITC (20.0 μg mL^{-1}) for 45 min. The samples were imaged using a laser confocal microscope (CLSM, Nikon A1R, Japan). The cells were washed with serum-free DMEM medium after 24 h incubation, fixed with 2.5% glutaraldehyde and dehydrated with ethanol solution of concentration gradient from 25% to 100%. After 24 h of air-dry treatment, the cell adhesion morphology was finally observed using a field emission scanning electron microscope (FESEM, Hitachi S-3400, Japan).

For the cell migration study, the sterilized nanofibrous films were placed into a 24-well plate, followed by the addition of DMEM solution according to the ISO-10993 standard. After the films were soaked for 24 h, the impregnating solution was taken out for further study. L929 cells were incubated with 0.5 mL of DMEM solution at a density of 2.0×10^4 cells per well in a 48-well plate and placed in a 37 °C incubator for cell confluence. Then, the cell-filled wells were scratched across their surface, followed by re-filling of the above sample impregnating solution containing 1.0% Gibco serum. After incubation for 24 h, cell migration behaviors were investigated using an optical microscope (Leica DMi8, Germany).

Wound healing assay

All animal models, laboratory procedures, and care were carried out in full approval of the Animal Care Committee of Shanghai Jiao Tong University Affiliated Sixth People's Hospital (Shanghai, China). 6–8 week old C57 mice were used to assess the effects of the samples on wound healing. After the mice were injected with anesthetic treatment, the hair on the backs of the mice was shaved. Two holes were made in the back of the mouse with a 5 mm diameter punch, followed by coverage with the biofilm samples or underwent no treatment (as control). After that, the wound was wrapped with a dressing mesh (3 M Healthy Care, 3590). After different treatment periods, the wound was unwrapped and imaged using a digital camera.

After 14 d treatment, the mice were sacrificed, and the wound tissues were removed, fixed, dehydrated, waxed, and sectioned by a tissue sectioner (Leica RM2265, Germany). The sectioned tissue slices then underwent hematoxylin-eosin (H&E) staining for histological examination using a fluorescent optical microscope (Leica DMi8, Germany).

The skin tissue sections were processed with immunohistochemical staining in order using Rabbit Anti-Collagen I antibody (Bioss, China) and goat anti-rabbit IgG (HRP) (Abacm, UK), and all procedures were performed according to the manufacturer's standards. Subsequently, they were developed with DAB reagent and counterstained with hematoxylin. Finally, the tissue section was placed under a fluorescent optical microscope (Leica DMi8, Germany).

The skin tissue sections were also immunohistochemically stained in order using Anti-CD31 Goat pAb (Servicebio, China) and rabbit anti-goat IgG (HRP) (Servicebio, UK), and all procedures were performed according to the manufacturer's standards. Subsequently, they were developed with DAB reagent and counterstained with hematoxylin. Finally, the tissue section was placed under the fluorescent optical microscope (Leica DMi8, Germany).

Statistical analysis

The statistical analysis was performed by SPSS Statistics 21.0 software. *P* values less than 0.05 were considered significant and all the results are presented as mean ± standard deviation.

Conflicts of interest

The authors declare no competing interests.

Acknowledgements

The research was supported by the National Key R&D Program of China (2018YFE0201500 and 2017YFB0309300), the National Natural Science Foundation of China (81772317 and 51973060), the National Natural Science Foundation of China for Innovative Research Groups (51621002) and the Frontiers Science Center for Materiobiology and Dynamic Chemistry. The funding grant from Shanghai International Cooperation Program (15520721200) is also acknowledged.

References

1 S. B. Mallik, B. S. Jayashree and R. R. Shenoy, *J. Diabetes Complicat.*, 2018, **32**, 524–530.

2 K. R. Jones, *Aging Health*, 2009, **5**, 851–866.
3 X. Hu, H. Zhang, X. Li, Y. Li and Z. Chen, *Wound Repair Regen.*, 2019, **28**, 6–15.
4 Y. J. Park, Y. Hwang, K. H. Park, J. W. Suh, D. W. Shim, S. H. Han, J. W. Lee and W. J. Choi, *Foot Ankle Orthopaedics*, 2016, **1**, 107861.
5 Y. Li, Y. Xiao and C. Liu, *Chem. Rev.*, 2017, **117**, 4376–4421.
6 F. Shohreh and A. Fatemeh, *Int. J. Pharm.*, 2019, **566**, 307–328.
7 M. Naseri-Nosar and Z. Ziora, *Carbohydr. Polym.*, 2018, **189**, 379–398.
8 I. Muhamed, E. Sproul, F. S. Ligler and A. C. Brown, *ACS Appl. Mater. Interfaces*, 2019, **11**, 3771–3780.
9 P. L. Thi, Y. Lee, D. L. Tran, T. T. H. Thi, J. I. Kang, K. M. Park and K. D. Park, *Acta Biomater.*, 2019, **103**, 142–152.
10 J. Devalliere, K. Dooley, Y. Yu, S. S. Kelangi, B. E. Uygun and M. L. Yarmush, *Biomaterials*, 2017, **141**, 149–160.
11 R. Atta, A. Sadia and I. Atif, *Carbohydr. Polym.*, 2019, **203**, 423–429.
12 S. Huang, T. Deng, Y. Wang, Z. Deng, L. He, S. Liu, J. Yang and Y. Jin, *Acta Biomater.*, 2008, **4**, 1057–1066.
13 C. Danielsson, S. Ruault, A. Basset-Dardare and P. Frey, *Biomaterials*, 2006, **27**, 1054–1060.
14 J. S. Boateng, K. H. Matthews, H. N. E. Stevens and G. M. Eccleston, *J. Pharm. Sci.*, 2008, **97**, 2892–2923.
15 H. Mndlovu, L. C. duToit, P. Kumar, T. Marimuthu, P. P. D. Kondiah, Y. E. Choonara and V. Pillay, *Carbohydr. Polym.*, 2019, **222**, 114988.
16 K. Cheirmadurai, P. Thanikaivelan and R. Murali, *Carbohydr. Polym.*, 2016, **137**, 584–593.
17 J. Wu, C. Li and C. Tsai, *Nanomedicine*, 2014, **5**, 1097–1107.
18 X. Yang, J. Yang, L. Wang, B. Ran, Y. Jia, L. Zhang, G. Yang, H. Shao and X. Jiang, *ACS Nano*, 2017, **11**, 5737–5745.
19 B. Kost, M. Svyntkivska, M. Brzeziński, T. Makowski, E. Piorkowska, K. Rajkowska, A. Kunicka-Styczyńska and T. Biela, *Colloids Surf., B*, 2020, **190**, 110949.
20 S. Chitrattha and T. Phaechamud, *Mater. Sci. Eng., C*, 2016, **58**, 1122–1130.
21 K. Ito, A. Saito, T. Fujie, K. Nishiwaki, H. Miyazaki, M. Kinoshita, D. Saitoh, S. Ohtsubo and S. Takeoka, *Acta Biomater.*, 2015, **24**, 87–95.
22 S. M. Davachi and B. Kaffashi, *Int. J. Polym. Mater. Polym. Biomater.*, 2015, **64**, 497–508.
23 S. P. Miguel, D. R. Figueira, D. Simoes, M. P. Ribeiro, P. Coutinho, P. Ferreira and I. J. Correia, *Colloids Surf., B*, 2018, **169**, 60–71.
24 Z. Piperigkou, M. Götte, A. D. Theocharis and N. K. Karamanos, *Adv. Drug Delivery Rev.*, 2018, **129**, 16–36.
25 A. R. Carvalho, R. M. Diniz, M. A. M. Suarez, C. S. S. E. S. Figueiredo, A. Zagmignan, M. A. G. Grisotto, E. S. Fernandes and L. C. N. da Silva, *Front. Pharmacol.*, 2018, **9**, 784.
26 T. Schreier, E. Degen and W. Baschong, *Res. Exp. Med.*, 1993, **193**, 195–205.
27 A. P. Veith, K. Henderson, A. Spencer, A. D. Sligar and A. B. Baker, *Adv. Drug Delivery Rev.*, 2019, **146**, 97–125.
28 L. E. Tracy, A. Raquel and E. J. Caterson, *Adv. Wound Care*, 2016, **5**, 119–136.
29 P. Bainbridge, *J. Wound Care*, 2013, **22**, 410–412.
30 D. Vianna, G. F. R. Teodoro, F. L. Torres-Leal and J. Tirapegui, *Braz. J. Pharm. Sci.*, 2010, **46**, 29–36.
31 H. Y. Bong, J. Y. Kim, H. I. Jeong, M. S. Moon, J. Kim and O. Kwon, *Nutr. Res. Pract.*, 2010, **4**, 106–113.
32 M. G. Pereira, M. T. Silva, F. M. Cunha, A. S. Moriscot, M. S. Aoki and E. H. Miyabara, *Exp. Gerontol.*, 2015, **72**, 269–277.
33 N. Wajih, X. Liu, P. Shetty, S. Basu, H. Wu, N. Hogg, R. P. Patel, C. M. Furdui and D. B. Kim-Shapiro, *Redox Biol.*, 2016, **8**, 415–421.
34 S. S. Ullrich, P. C. Fitzgerald, G. Schober, R. E. Steinert, M. Horowitz and C. Feinlebisset, *Am. J. Clin. Nutr.*, 2016, **104**, 1274–1284.
35 D. Kalogeropoulou, L. LaFave, K. Schweim, M. C. Gannon and F. Q. Nuttall, *Metabolism*, 2008, **57**, 1747–1752.
36 C. J. Hu, F. N. Li, Y. H. Duan, Y. L. Yin and X. F. Kong, *Front. Microbiol.*, 2019, **10**, 1767–1779.
37 D. Vianna, G. F. T. Resende, F. L. Torres-Leal, L. C. Pantaleo, J. D. Donato and J. Tirapegui, *Nutrition*, 2012, **28**, 182–189.
38 A. Kelly, C. Li, Z. Gao, C. A. Stanley and F. M. Matschinsky, *Diabetes*, 2002, **51**, S421–S426.
39 E. M. Gonçalves and M. C. C. G. Marcondes, *Front. Microbiol.*, 2019, **38**, 145–153.
40 R. L. Wolfson, L. Chantranupong, R. A. Saxton, K. Shen, S. M. Scaria, J. R. Cantor and D. M. Sabatini, *Science*, 2016, **351**, 43–48.
41 C. Gopalan and S. G. Srikantia, *Lancet*, 1960, **1**, 954–957.
42 S. E. Koch, S. Packman, T. K. Koch and M. L. Williams, *J. Am. Acad. Dermatol.*, 1993, **28**, 289–292.
43 M. Diba, F. Tapia, A. R. Boccaccini and L. A. Strobel, *Int. J. Appl. Glass Sci.*, 2012, **3**, 221–253.
44 X. Wang, L. Gao, Y. Han, M. Xing, C. Zhao, J. Peng and J. Chang, *Adv. Sci.*, 2018, **5**, 1800776.
45 E. Lizundia, E. Meaurio, J. M. Laza, J. L. Vilas and L. M. León Isidro, *Mater. Sci. Eng., C*, 2015, **50**, 97–106.
46 Y. Yang, X. Qiu, Y. Sun, Y. Wang, J. Wang, Y. Li and C. Liu, *R. Soc. Open Sci.*, 2018, **5**, 170868.
47 J. L. Daristotle, A. M. Behrens, A. D. Sandler and P. Kofinas, *ACS Appl. Mater. Interfaces*, 2008, **4**, 1057–1066.
48 A. M. Behrens, B. J. Casey, M. J. Sikorski, K. L. Wu, W. Tutak, A. D. Sandler and P. Kofinas, *ACS Macro Lett.*, 2014, **3**, 249–254.
49 Y. A. Ivanenkov, A. E. Machulkin, A. S. Garanina, D. A. Skvortsov, A. A. Uspenskaya, E. V. Deyneka, A. V. Trofimenko, E. K. Beloglazkina, V. E. K. N. V. Zyk, D. S. Bezrukov, A. V. Aladinskaya, N. S. Vorobyeva, M. M. Puchinina, G. K. Riabykh, A. A. Sofronova, A. S. Malyshev and A. G. Majouga, *Bioorg. Med. Chem. Lett.*, 2019, **29**, 1246–1255.
50 P. Kensbock, D. E. Demco, S. Singh, K. Rahimi, R. Fechete, A. Walther, A. M. Schmidt and M. Möller, *Langmuir*, 2016, **33**, 66–74.
51 L. Bippus, M. Jaber and B. Lebeau, *New J. Chem.*, 2009, **33**, 1116–1126.
52 N. A. A. Razak, A. H. Ahmad and T. Winie, *AIP Conf. Proc.*, 2009, **1136**, 21–25.
53 R. Wu, C. Ma, Y. Liang, F. Chen and X. Liu, *Appl. Mater. Today*, 2020, **18**, 100508.

54 D. Mao, Q. Li, N. Bai, H. Dong and D. Li, *Carbohydr. Polym.*, 2018, **180**, 104–111.
55 Y. Arima and H. Iwata, *Biomaterials*, 2007, **28**, 3074–3082.
56 H. Y. Chang, C. C. Huang, K. Y. Lin, W. L. Kao, H. Y. Liao, Y. W. You, J. H. Lin, Y. T. Kuo, D.-Y. Kuo and J. J. Shyue, *J. Phys. Chem. C*, 2014, **118**, 14464–14470.
57 P. Saini, M. Arora and R. M. N. V. Kumar, *Adv. Drug Delivery Rev.*, 2016, **107**, 47–59.
58 Y. Zhan, M. Goncalves, P. Yi, D. Capelo, Y. Zhang, J. Rodrigues, C. Liu, H. Tomas, Y. Li and P. He, *J. Mater. Chem. B*, 2015, **3**, 4221–4230.
59 K. Zhang, H. Zheng, S. Liang and C. Gao, *Acta Biomater.*, 2016, **37**, 131–142.
60 S. H. Oh, I. K. Park, J. M. Kim and J. H. Lee, *Biomaterials*, 2007, **28**, 1664–1671.
61 B. Wang, P. Zhang, W. Song, L. Zhao and C. He, *J. Ind. Text.*, 2016, **45**, 516–530.
62 S. Sipahi, O. Gungor, M. Gunduz, M. Cilci, M. C. Demirci and A. Tamer, *BMC Nephrol.*, 2013, **14**, 8–14.
63 Y. Luo, H. Shen, Y. Fang, Y. Cao, J. Huang, M. Zhang, J. Dai, X. Shi and Z. Zhang, *ACS Appl. Mater. Interfaces*, 2015, **7**, 6331–6339.
64 R. Lakshmanan, P. Kumaraswamy, U. M. Krishnan and S. Sethuraman, *Biomaterials*, 2016, **97**, 176–195.
65 R. Singla, S. Soni, V. Patial, P. M. Kulurkar, A. Kumari, S. Mahesh, Y. S. Padwad and S. K. Yadav, *Int. J. Biol. Macromol.*, 2017, **105**, 45–55.
66 H. Xie, X. Chen, X. Shen, Y. He, W. Chen, Q. Luo, W. Ge, W. Yuan, X. Tang, D. Hou, D. Jiang, Q. Wang, Y. Liu, Q. Liu and K. Li, *Int. J. Biol. Macromol.*, 2018, **107**, 93–104.
67 C. Dunnill, T. Patton, J. Brennan, J. Barrett, M. Dryden, J. Cooke, D. Leaper and N. T. Georgopoulos, *Int. Wound J.*, 2017, **14**, 89–96.

